Low-cost GNSS/INS integration for enhanced land vehicle performance

Chao Chen and Guobin Chang[1]

Key Laboratory of Land Environment and Disaster Monitoring of Ministry, MNR, China University of Mining and Technology, Xuzhou 221116, People's Republic of China
School of Environmental Science and Spatial Informatics, China University of Mining and Technology, Xuzhou 221116, People's Republic of China

E-mail: guobinchang@hotmail.com (G Chang)

CrossMark

Abstract
An enhanced integrated navigation algorithm was developed to fuse the time-differenced global navigation satellite system (GNSS) carrier phase and inertial navigation system (INS) measurements to enhance land vehicle performance. The proposed algorithm aims to enhance a system's reliability and availability for a low-cost single-frequency GNSS receiver and low-accuracy INS, thereby improving the system's performance in GNSS-challenged environments. A rigorous stochastic model for the time-differenced carrier phase (TDCP) measurement noise is constructed and colored noises of a special type are found. This approach avoids over-optimistic estimation and improves the transient accuracy of the estimates. Given that TDCP is a relative measurement, the position error of the TDCP-INS coupled system will not converge. To bound the position error drift of the TDCP-INS and suppress the INS position drift during GNSS outages, a non-holonomic constraint and odometer measurements are incorporated into the integrated system. Vehicular tests have been conducted in suburban and urban areas to evaluate the performance of the proposed TDCP-INS tightly coupled system. The result demonstrates the effectiveness of the proposed algorithm at reducing the position drift of the TDCP-INS and suppressing error accumulation during GNSS outages compared with the traditional TDCP-INS and SPP-INS tightly coupled navigation system.

Keywords: integrated navigation, GNSS, INS, TDCP, NHC

(Some figures may appear in colour only in the online journal)

1. Introduction

The inertial navigation system (INS) with a global navigation satellite system (GNSS) is no longer new in the field of modern navigation systems [1–5]. A GNSS and INS coupled system can incorporate the benefits of the two systems and overcome their individual deficiencies. In particular, GNSS and INS integration can provide long-term highly accurate solutions when GNSS signals are normal, and provide coasting ability to bridge GNSS outages [6] when GNSS signals are blocked [7]. Motivated by the distinctively complementary technology of the GNSS and INS, integration has been widely investigated to improve the navigation performance over the past decade. From the perspective of the GNSS positioning mode, the types of tightly coupled integration systems can be summarized as: (1) INS aiding single point positioning (SPP-INS)-based pseudo-ranges (PRs) [7], (2) INS aiding SPP-based time-differenced carrier phases (TDCP-INS) [8, 9], (3) INS aiding real-time kinematic (RTK-INS)-based double-differenced PRs and carrier phases (CPs) [10, 11], and (4) INS aiding precise point positioning (PPP-INS)-based zero-differenced PRs and CPs [12, 13].

The RTK-INS system can achieve centimeter-lever positioning accuracy with ambiguities correctly fixed to integers [12]. However, the needed reference stations increase the system's cost, and the limited working distance weakens

[1] Author to whom any correspondence should be addressed.

the application of the RTK-INS system [14]. Moreover, an ambiguity resolution (AR) process strategy under a GNSS-challenged environment should be considerably robust because of ill-conditioning of the normal equations [15]. Hence, additional information, such as baseline length constraint [16], atmospheric constraint [17], or partial AR strategy [18], could improve the success and efficiency of the AR process. Evidently, the AR process is not only a complex problem in RTK-based applications but also in GNSS-INS tightly coupled systems, particularly under severe environments for single-frequency users.

SPP-INS, TDCP-INS, and PPP-INS systems belong to the category of a single station mode. Decimeter-level positioning accuracy can be obtained with the PPP-INS system with additional precise products and a rigorous error model [13]. However, such a work is complex. Hence, obtaining high-accuracy navigation solutions should pay the price and costs in reliability or complexity. The SPP-INS system has the advantages of low-cost, low calculation load, and easy real-time operation. However, only several meters of positing solutions can be achieved because of large PR noises. Thus, the SPP-INS system suitable for a low-cost GNSS receiver and inertial equipment based on a micro-electro-mechanical system (MEMS) for land vehicle navigation applications [19] does not require high-accuracy positioning solutions.

CP measurements are highly precise but ambiguous, whereas PR measurements are simple (direct distance) but with large noises. The TDCP measurement is precise and unambiguous, but the current TDCP measurement is linearly connected to the previous and current position states. The time-differenced operation brings about time correlations between measurements at consecutive epochs [20]. If these time correlations are disregarded, then the estimator will work with an incorrect stochastic model, thereby resulting in loss of precision in parameter estimation and inconsistent accuracy evaluation [21]. An INS aiding a TDCP can substantially improve the navigation performance of an integrated system [7–9], thereby leading to a compromise acceptable to CPs (precision) and PRs (simplicity). The two different categories of the TDCP and INS integrated method are position constraint (PC)-based [9] and velocity constraint (VC)-based [7, 8, 22], which have pros and cons as different approximation methods. The two methods are theoretically equivalent. For the VC-TDCP-INS, TDCPs are viewed as a function of velocity. Accordingly, velocity is an estimated state in the measurement update of the Kalman filter (KF). This method is a rigorous derivate, but low filtering performance will be caused by complex integral operation and matrix exponentiation. For the PC-TDCP-INS, the assumption is that the position state at the previous epoch is known. Thereafter, TDCPs can be recovered to PRs to estimate the current position state. This method is as simple as SPP-INS. However, the residual position errors at a previous epoch should be taken seriously in the random model. INS and TDCP measurements only carry relative position information, and the position drift of the integration system cannot be bounded. Thus, the TDCP-INS system can only achieve short-term excellent performance and will introduce long-term position error accumulation.

To bound the position drift, PRs can be augmented as observations in the KF toward achieving an absolution estimation [22]. However, only the SPP-level accuracy can be achieved by PRs with a TDCP-INS tightly coupled navigation system [7, 23]. Therefore, special considerations are required to provide accurate absolutions for the TDCP-INS system. One direct method involves adding other absolute sensors, such as a built-in odometer (ODO), magnetic compass, and GNSS dual antennas, to bound the increasing positioning errors of the TDCP-INS system. This approach is relatively effective but involves other costs, which are not affordable for many low-end land-based navigation systems [24, 25]. To enhance the low-end land-based vehicle navigation performance, non-holonomic constraint (NHC) is the most typical enhancement algorithm [5]. Unless the vehicle jumps off or slides on the ground, the velocity of the vehicle in the plane perpendicular to the forward direction is nearly zero in this algorithm [24]. Thus, NHC can provide alternative velocity constraint information and an auxiliary sensor, such as ODOs, can provide velocity solutions to overcome performance limitations in GNSS-challenged environments [1, 26].

An enhanced TDCP-INS integrated navigation system is proposed by combining the aforementioned two aspects. Two major goals of this work are to: (1) propose a simple but rigorous TDCP-INS tightly coupled system, and (2) use an NHC derived from the vehicle motion model. Meanwhile, the ODO-derived speed can be integrated into the TDCP-INS system to bound the position drift and enhance vehicle navigation performance in GNSS-challenged environments.

The remainder of this paper is organized as follows. The TDCP measurement models are introduced first. Thereafter, the conventional INS error models in the navigation frame and architectures for the TDCP-INS coupled system are presented. The NHC based on the vehicle motion properties and velocity observations from the built-in ODO are briefly described. Lastly, the performance of the proposed scheme is evaluated by vehicular tests conducted in suburban and urban areas.

2. TDCP-INS integration algorithm

The linearized carrier phase observation and TDCP measurement equation are first derived. Thereafter, the INS error equations and NHC algorithm are introduced. Lastly, the TDCP-INS integrated system is presented.

2.1. TDCP equations

The linearized equation of original observations is written as follows [27]:

$$L_k = \boldsymbol{\mu}_k \delta \boldsymbol{p}_k + r_{0,k} + t_{\mathrm{r},k} - t_k^{\mathrm{s}} + T_k - I_k + \lambda N + \xi_k \quad (1)$$

where the indices k refer to the satellite and epoch, respectively; L denotes the observed minus computed values of CP observables; $\boldsymbol{\mu}$ is the unit vector of the component from the receiver to the satellite; $\delta \boldsymbol{p}$ is the vector of the receiver position increments relative to the priori position; r_0 is the approximate distance between the satellite and receiver; t_{r} and t^{s} are

INS Mech.   refer to   INS Mechanization
Meas. Upd   refer to   Measurement Update
Vel. Info.   refer to   Velocity Information
Vel. Const. refer to   Velocity Constraint
CS Dete.   refer to   Cycle Slip Detection
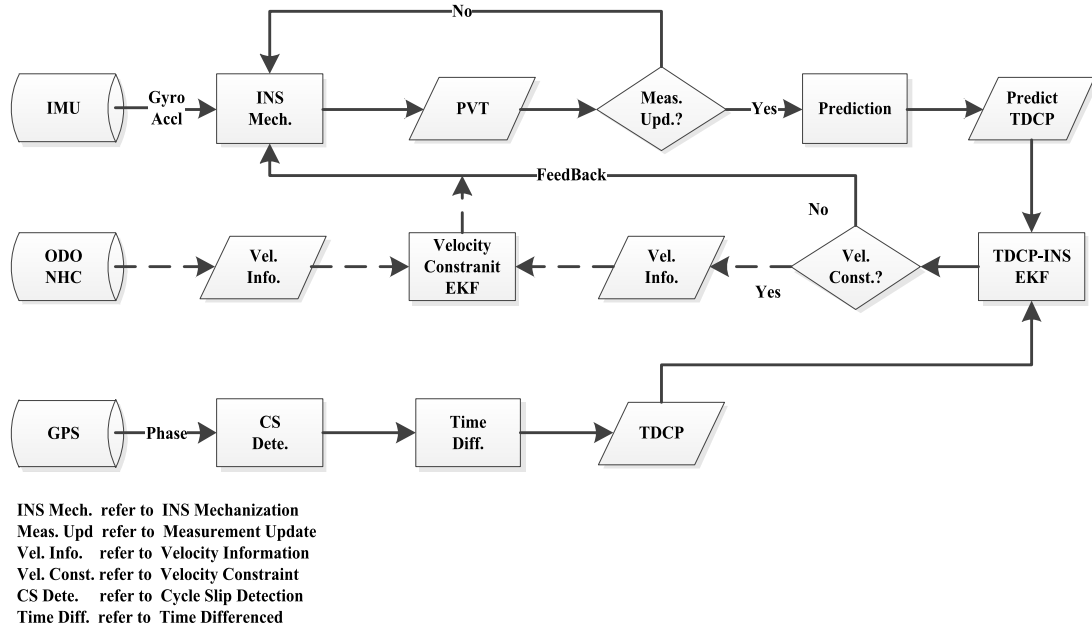**Time Diff.   refer to   Time Differenced**

Figure 1. A flowchart of the proposed TDCP-INS integration scheme with velocity aiding.

the receiver and satellite clock offsets, respectively; T and I denote the troposphere and ionosphere delays, respectively; λ is the carrier wavelength; N is the integer phase ambiguity; and ξ is the measurement noise for the CP observations.

The time-differenced operator of the CP can eliminate the constant integer ambiguity and the majority of the common errors introduced by the tropospheric, ionospheric, and ephemeris conditions because they vary gradually within a small sampling rate [9]. TDCP measurement can be formulated as follows using equation (1):

$$
\begin{aligned}
\mathrm{d}L_k &= L_k - L_{k-1} \\
&= (r_{0,k} + \boldsymbol{\mu}_k \delta \boldsymbol{p}_k + t_{\mathrm{r},k} - t_k^{\mathrm{s}}) \\
&\quad - (\hat{r}_{k-1} + \boldsymbol{\mu}_{k-1} \delta \hat{\boldsymbol{p}}_{k-1} + \hat{t}_{\mathrm{r},k-1} - t_{k-1}^{\mathrm{s}}) + \xi_k - \xi_{k-1} \\
&= \boldsymbol{\mu}_k \delta \boldsymbol{p}_k + t_{r,k} + (r_{0,k} - t_k^{\mathrm{s}} - \hat{r}_{k-1} - \hat{t}_{\mathrm{r},k-1} + t_{k-1}^{\mathrm{s}}) + d\xi_k
\end{aligned}
\tag{2}
$$

where d denotes the time-differenced operator; the variable with a leading δ denotes the error and a variable with $\hat{}$ denotes the posterior estimate; $\mathrm{d}L_k$ denotes the TDCP observation of the satellite at epoch k; $\hat{r}_{k-1}$ denotes the posterior range calculated by the posterior position estimate $\hat{\boldsymbol{p}}_{k-1}$; and $\delta \hat{\boldsymbol{p}}_{k-1}$ denotes the estimate error. Moreover, (1) $\mathrm{d}L$ only carries relative information and does not contain absolute positioning information, (2) the positioning accuracy of the TDCP is achieved at a float-solution level at most, (3) the positioning error of the TDCP will accumulate by $\delta \hat{\boldsymbol{p}}_{k-1}$, and (4) the covariance matrix between $\delta \hat{\boldsymbol{p}}_{k-1}$ and $\mathrm{d}\xi_k$ may not be zero in general.

To simplify, the satellite clock offset is corrected by ephemeris, and the receiver clock is eliminated by satellite difference. Hence, a new variable is defined from equation (2) as follows:

$$
\begin{aligned}
y_k &= \nabla \mathrm{d}L_k + \nabla \hat{r}_{k-1} - \nabla r_{0,k} \\
&= \nabla \boldsymbol{\mu}_k \delta \boldsymbol{p}_k + \nabla \boldsymbol{\mu}_{k-1} \delta \hat{\boldsymbol{p}}_{k-1} + \nabla d\xi_k \\
&= \nabla \boldsymbol{\mu}_k \delta \boldsymbol{p}_k + \varsigma_k
\end{aligned}
\tag{3}
$$

Table 1. The specifications of the IMU.

Specifications	Gyroscopes	Accelerometers
Bias	$1 \,^\circ \mathrm{h}^{-1}$	1 mg
Bias Stability	$0.1 \,^\circ \mathrm{h}^{-1}$	1 µg
White Noise	$0.15 \,^\circ \mathrm{sqrt(h)}^{-1}$	55 µg sqrt(Hz)$^{-1}$

where ∇ denotes the satellite difference operator. Here, y_k denotes the observed minus computed (OMC) values for TDCP observables at epoch k, and ς_k denotes the sum of the measurement noise and posterior estimate error.

Assuming n satellites are simultaneously tracked, equation (3) can be rewritten as follows:

$$
\boldsymbol{y}_k = \boldsymbol{H}_k \delta \boldsymbol{p}_k + \varsigma_k
\tag{4}
$$

$$
\begin{aligned}
\mathrm{cov}\left[\varsigma_k, \varsigma_k^T\right] &= \boldsymbol{H}_{k-1} \boldsymbol{Q}_{\hat{p}\hat{p},k-1} \boldsymbol{H}_{k-1}^T + \boldsymbol{Q}_{\xi\xi,k} \\
&\quad + \boldsymbol{Q}_{\xi\xi,k-1} - \boldsymbol{H}_{k-1} \boldsymbol{C}_{k-1} - \boldsymbol{C}_{k-1}^T \boldsymbol{H}_{k-1}^T
\end{aligned}
\tag{5}
$$

$$
\begin{aligned}
\boldsymbol{C}_k &= \mathrm{cov}\left[\delta \hat{\boldsymbol{p}}_k, \boldsymbol{H}_k \delta \hat{\boldsymbol{p}}_k + \varsigma_k\right] \\
&= Q_{\hat{p}\hat{p},k} \boldsymbol{H}_k^T \boldsymbol{Q}_{\varsigma\varsigma,k}^{-1} \boldsymbol{Q}_{\xi\xi,k}
\end{aligned}
\tag{6}
$$

where $\boldsymbol{H}_k$ denotes the measurement matrix; $\boldsymbol{Q}_{\xi\xi,k}$, $\boldsymbol{Q}_{\hat{p}\hat{p},k}$ denotes the CP measurement variance matrix and posterior position estimate variance, respectively; and $\boldsymbol{Q}_{\varsigma\varsigma,k}$ denotes the TDCP measurement variance matrix.

Equations (4)–(6) are fundamental formulas of the TDCP observations. Equation (4) indicates that relative TDCP measurement can recover to PR. Thus, the TDCP-based positioning mode can be operated as SPP mode. Equation (5) gives the correlation of the TDCP measurement error, which can be found in the last two terms on the right-hand side of equation (5). Then, the estimator will work with an incorrect stochastic model, thereby resulting in loss of precision in parameter estimation and inconsistent accuracy evaluation. Equation (6)

shows that C_k should be calculated and stored in the memory at each epoch, and C_0 can be set as zero.

2.2. INS equations

The mechanization equation is a process involving converting the output of an INS into position, velocity, and attitude information when the initial conditions of the system are known. The details of the mechanization equations are available in [2]. The INS error equations obtained by linearizing the mechanization equations in the n-frame can be summarized as follows:

$$
\begin{cases}
\dot{\psi}^n = -\omega_{in}^n \times \psi^n - C_b^n \varepsilon^b \\
\delta \dot{v}^n = -\left(C_b^n f^b\right) \times \psi^n - \left(\omega_{ie}^n + \omega_{in}^n\right) \times \delta v^n + \delta g^n + C_b^n \nabla^b \\
\delta \dot{p}^n = -\omega_{in}^n \times \psi^n + \delta \dot{v}^n
\end{cases}
\tag{7}
$$

where the superscripts i and b denote the inertial and body frame (i-frame and b-frame), respectively; ω_{yz}^x denotes the rotation rate of the y-frame relative to the z-frame expressed in the x-frame; ψ^n, δv^n, and δp^n are the attitude, velocity, and position error vectors, respectively; ω_{en}^n is the rotation vector from the e-frame to the n-frame; f^b is the specific force vector; δg^n is the error of the gravity vector in the n-frame; C_b^n is the transition matric from the b-frame to the n-frame; and ∇^b and ε^b are the accelerometer and gyro drift vector, respectively, expressed in the b-frame.

2.3. Velocity aiding

NHC based on the vehicle motion model is implemented [19]. Unless the vehicle jumps off the ground or slides on the ground, the velocity of the vehicle in the plane perpendicular to the forward direction is nearly zero [1]. If the b-frame selects a right-front-up form, two NHCs can be considered as the measurement update of the KF. Meanwhile, the vehicle speed v_o can be obtained from the built-in ODO. The preceding assumption can be simplified and described mathematically as follows [19]:

$$
\begin{cases}
v_x^b \sim N\left(0, \sigma_x^2\right) \\
v_y^b \sim N\left(v_0, \sigma_y^2\right) \\
v_z^b \sim N\left(0, \sigma_z^2\right)
\end{cases}
\tag{8}
$$

The equation that relates the velocity in the b-frame to the n-frame is as follows:

$$
v^b = C_n^b v^n. \tag{9}
$$

Perturbing the upper equation and collecting terms to the first order provides the following equation:

$$
\delta v^b = C_n^b \delta v^n + C_n^b v^n \times w_{nb}^n \tag{10}
$$

where v and δv denote the velocity and velocity error vector, respectively, and C_b^n is the transition matrix from the n-frame to the b-frame. From equations (8) and (9), the measurement equations can be constructed as follows:

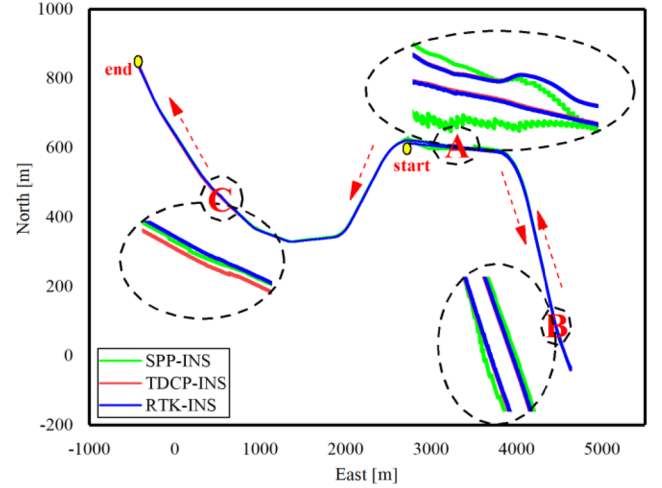**Figure 2.** Reference trajectory indication. Map data: Google, Maxar Technologies.

Figure 3. The 2D vehicle trajectory for the SPP-INS (green), TDCP-INS (red), and RTK-INS (blue).

$$
y_v = \begin{bmatrix} 0 \\ v_o \\ 0 \end{bmatrix} - C_n^b v^n \tag{11}
$$

$$
H_v = \left[C_n^b v^n \times, C_n^b, 0, 0, 0\right]_{3 \times 15}.
$$

The extending KF (EKF) is the most widely used estimator for fusing multi-sensor observations. The EKF consists of two parts, namely the system and measurement models, which are given in equation (12)(more details can be found in [2]):

$$
\begin{cases}
\delta x_k^- = F_{k,k-1} \delta \hat{x}_{k-1}^+ \\
P_k^- = F_{k,k-1} P_{k-1}^+ F_{k,k-1}^T + Q_{k-1} \\
K_k = P_k^- H_k \left(H_k P_k^- H_k^T + R_k\right) \\
\delta \hat{x}_k^+ = \delta x_k^- + K_k \left(y_k - H_k \delta x_k^-\right) \\
P_k^+ = \left(I - K_k H_k\right) P_k^-
\end{cases}
\tag{12}
$$

For the TDCP-INS tightly coupled KF, the system model, namely the state transition matrix $F_{k,k-1}$, is obtained from the INS error in equation (7) and extern states vector for accelerometer and gyro bias; both are modeled as first-order Markov processes. Thus, the estimated states can be noted as:

$$
\delta x = [\phi, \delta v, \delta p, b_a, b_g]^T. \tag{13}
$$

The measurement model, namely H_k, is obtained from equations (4)–(6) by augmenting with new error states.

For the velocity-aiding KF, the system model, namely the state transition matrix $F_{k,k-1}$, can be found in equation (10)
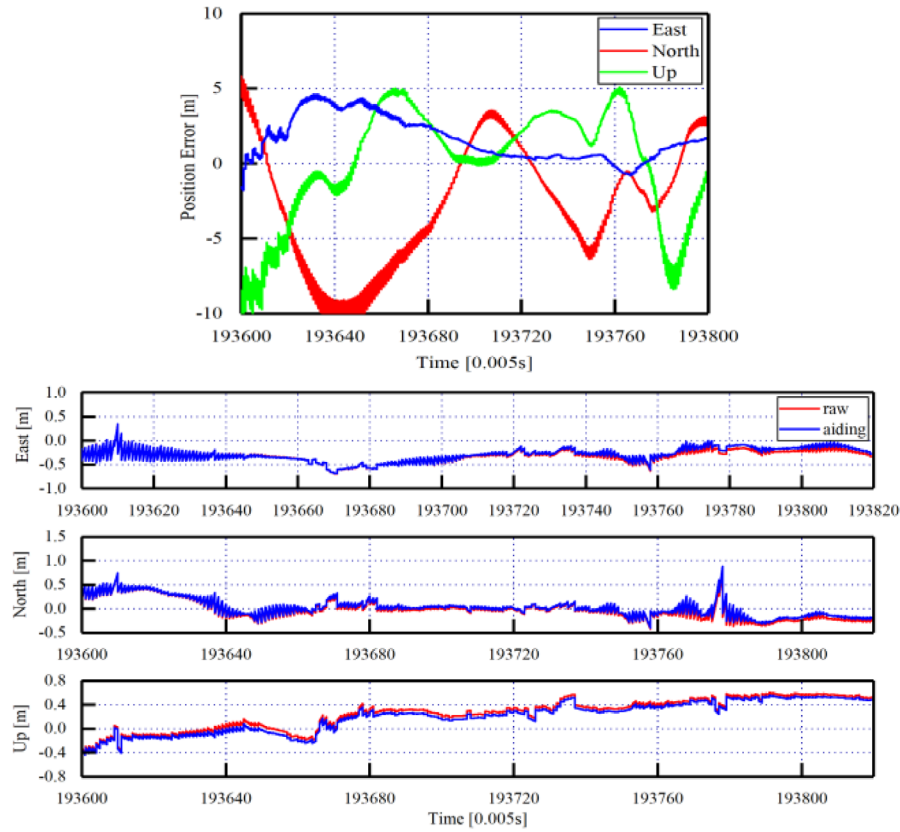
Figure 4. Position differences of the SPP-INS (top) and TDCP-INS (bottom) solutions with respect to the reference solution using the RTK-INS tightly coupled system.

and the estimated states are the same as shown in equation (13). The measurement, namely $\boldsymbol{H}_k$, is obtained from equation (11). Figure 1 shows the flowchart of the proposed TDCP-INS integration schemes with velocity aiding.

3. Experimental result

To access the performance of the proposed algorithm compared with the conventional SPP-INS, two field tests were conducted in November 2017 in the urban areas of Wuhan. For these tests, the output rate of the Inertial Measurement Unit (IMU) was configured as 200 Hz. The specifications of the IMU are presented in table 1. Trimble's R9 dual-frequency receivers were used at the rover and base stations for collection of raw GPS data at a rate of 1 Hz.

3.1. Overall performance test

The first data set was collected with a static initialization period of 5 min. The vehicle experiences several motion scenarios, such as turning, accelerating, and long driving. Figure 2 shows the trajectory.

The data were processed with three schemes: (1) SPP-INS, (2) TDCP-INS, and (3) RTK-INS. In the validation, the solutions from the dual-frequency multi-constellation RTK-INS tightly coupled system were used as a reference. Figure 3 shows the 2D vehicle trajectory for the SPP-INS system

(green), TDCP-INS system (red), and RTK-INS system (blue). A, B, and C denote the partial enlargement.

At the starting moment (see the partially enlarged A in figure 3), the SPP-INS tightly coupled navigation system can only achieve SPP accuracy (several meters). Compared with the SPP-INS, the TDCP-INS system was able to track the dynamics of the vehicle smoothly and was closely compared to the reference solutions. The TDCP-INS can achieve sub-meter positioning accuracy. At the intermediate moment (see the partially enlarged B), the SPP-INS and TDCP-INS solutions became steady. However, the TDCP-INS performed better than the SPP-INS. However, the TDCP measurements only carried relative positioning information, which will introduce position error accumulation without absolute position aiding. This phenomenon is shown in the partially enlarged C. As expected, the solutions from the SPP-INS approximate the reference solution. This result is evident proof of the disadvantage of the TDCP-INS compared with the SPP-INS.

3.2. Sky field-of-view test

For accuracy, data over the period from 193 600 s to 193 800 s with reasonable GPS continuity were processed. The dual-frequency RTK-INS solutions with full ambiguities-fixed were used as the reference trajectory to evaluate the solutions, which were accurate to a few centimeters. The duration of this field test was 200 s (total 40 000 epochs). Three schemes were considered to demonstrate the improvement of the TDCP-INS
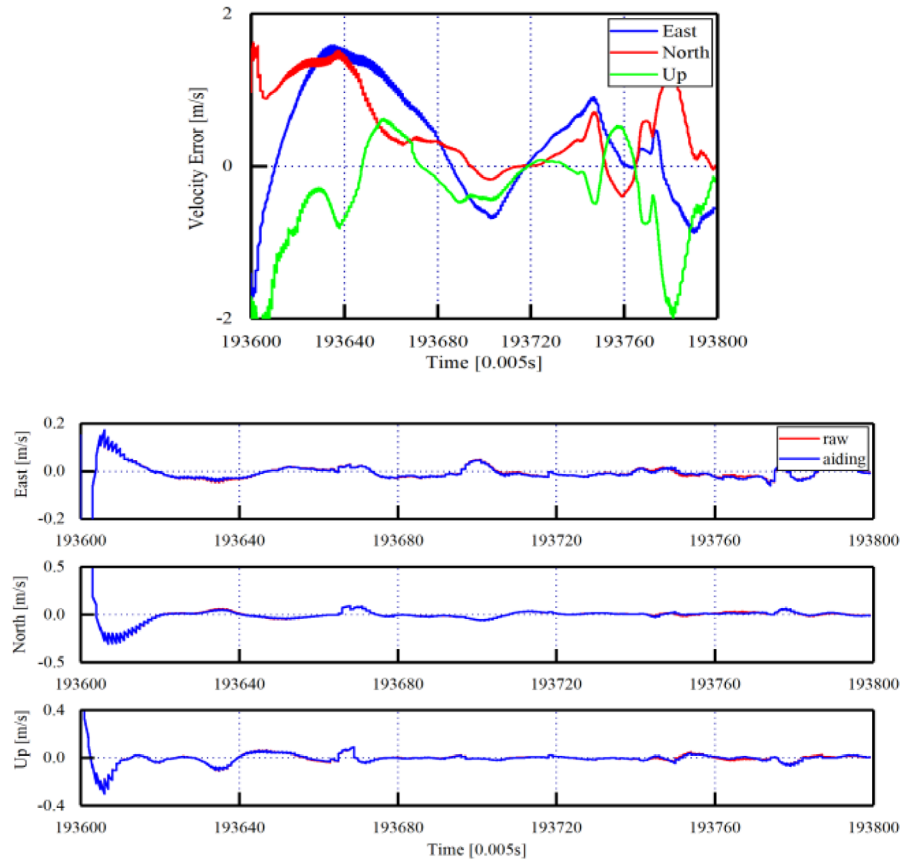
Figure 5. Velocity differences of the SPP-INS (top) and TDCP-INS (bottom) solutions with respect to the reference solution using the RTK-INS tightly coupled system.

Table 2. The RMSE of the position, velocity, and attitude of the three processing schemes with respect to the reference solution using the RTK-INS tightly coupled system under the sky field-of-view environment.

Mode	Position (m)			Velocity (m s^{-1})			Attitude (deg)		
	East	North	Up	East	North	Up	Roll	Pitch	Yaw
SPP-INS	2.1319	3.6533	4.7239	1.3004	1.2912	1.5562	0.5260	0.5412	5.6237
TDCP-INS	0.3653	0.1866	0.3595	0.0825	0.1209	0.1453	0.1432	0.1055	1.2354
TDCP-INS aiding	0.3365	0.1549	0.3463	0.0820	0.1204	0.1450	0.1411	0.1008	1.2305

and velocity-aiding methods: (1) the SPP-INS tightly coupled system, (2) the proposed TDCP-INS tightly coupled system (raw), and (3) the TDCP-INS tightly coupled system with velocity-aiding (blue). The constraints are augmented to the KF measurement model as pseudo-velocity measurements with the covariance derived from the misalignment angles based on the error propagation law [1, 19].

Table 1 shows the root mean square error (RMSE) of the differences in position, velocity, and attitude derived with the SPP-INS, TDCP-INS, and TDCP-INS with velocity aiding with the reference solution. Figures 4–6 show the time series of the position, velocity, and attitude differences, respectively. As expected, the position, velocity, and attitude RMSE of the TDCP-INS were better than those of the SPP-INS, and the positioning accuracy has increased by an order of magnitude. This navigation performance difference is attributed to using high-accuracy CP measurements. Moreover, the computational efficiency of the TDCP-INS is

equal to that of the SPP-INS. The relative CP measurements are converted to absolute PR measurements with some error accumulation in the TDCP-INS. Evidently, the TDCP-INS with velocity aiding showed a smaller position drift in the same scenario. Subsequently, the absolute positioning accuracy was improved. NHC assumes that the velocity of the vehicle in the plane perpendicular to the forward direction is zero. This information can perform as absolute aiding observations, such as the PR. Meanwhile, the ODO provides additional velocity measurement to aid the TDCP-INS. Through error propagation, the additional velocity-aiding information can bound the position drift of the TDCP-INS system (see figure 4). The statistics shown in table 1 indicate that the positions of the RMSE in the east, north, and up directions have improved from 0.3653, 0.1866, and 0.3595 m of the TDCP-INS to 0.3365, 0.1549, and 0.3463 m of the TDCP-INS with the velocity-aiding solution with improvements of 7.8%, 17.0%, and 3.7%, respectively.
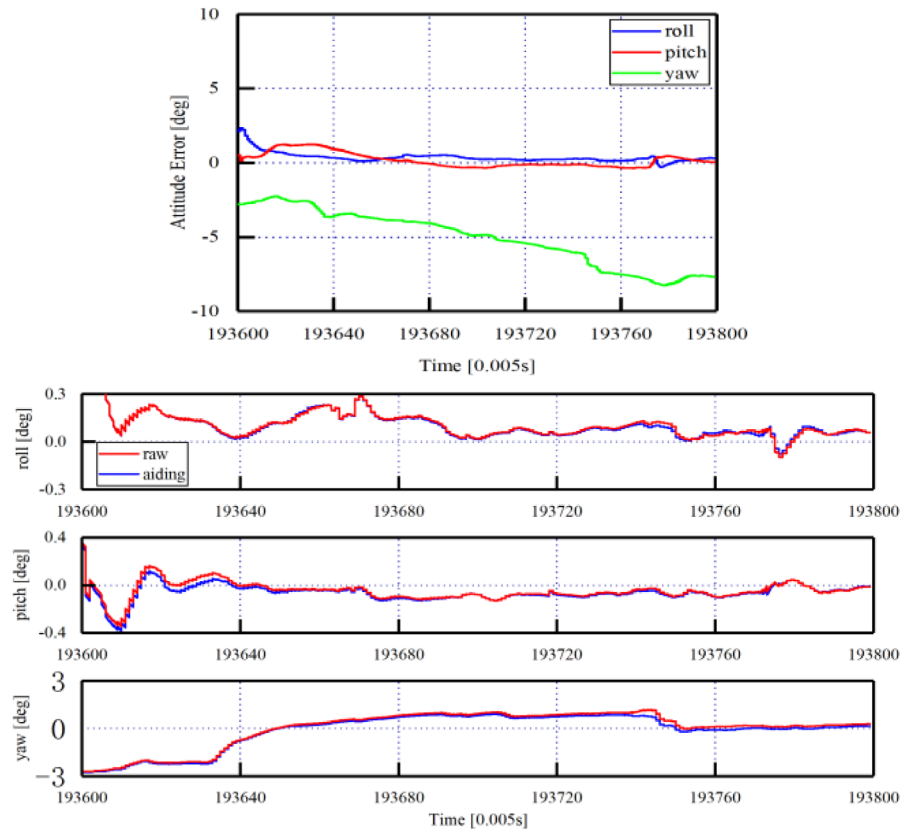
Figure 6. Attitude differences of the SPP-INS (top) and TDCP-INS (bottom) solutions with respect to the reference solution using the RTK-INS tightly coupled system.
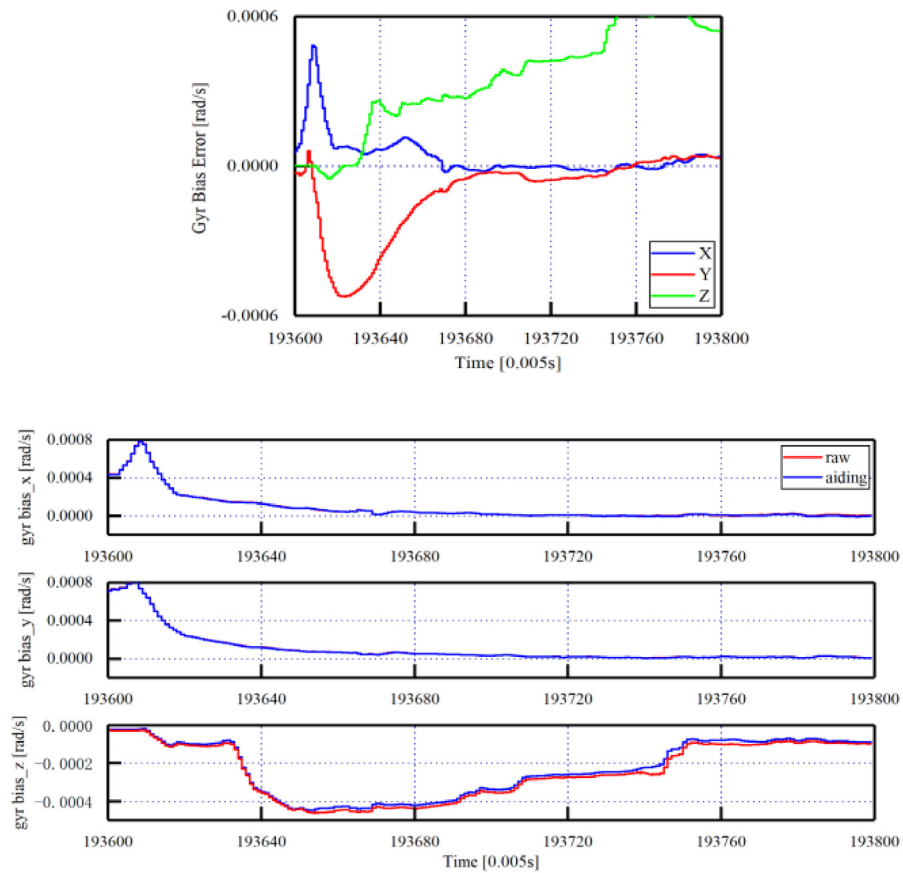

Figure 7. Estimated gyro bias differences of the SPP-INS (top) and TDCP-INS (bottom) solutions with respect to the reference solution using the RTK-INS tightly coupled system.
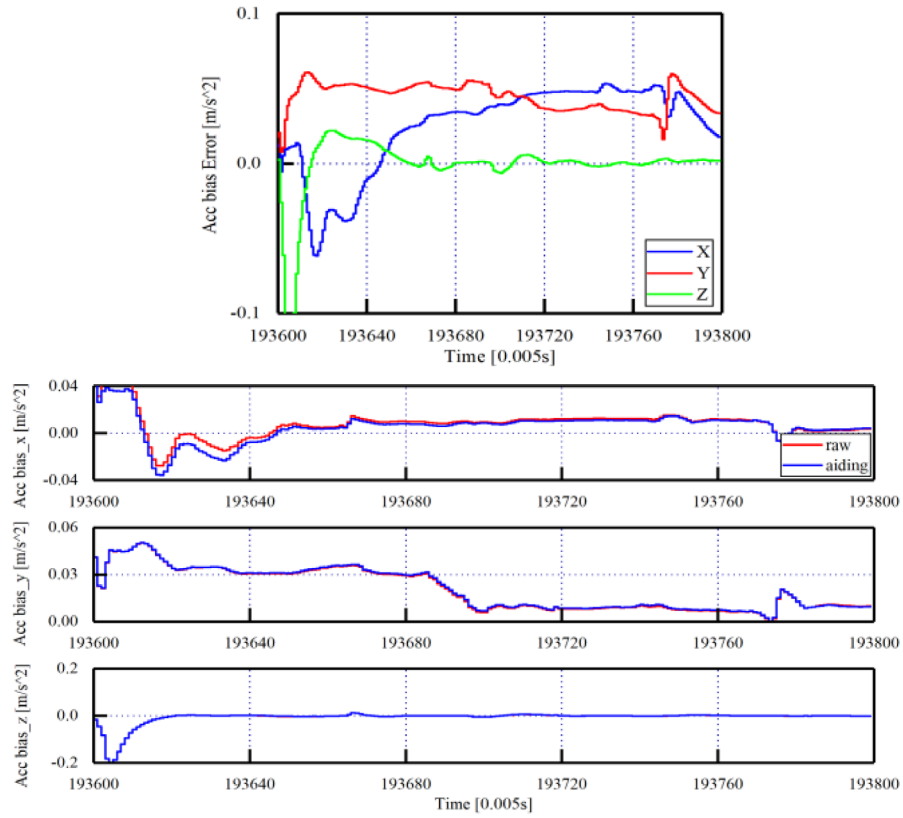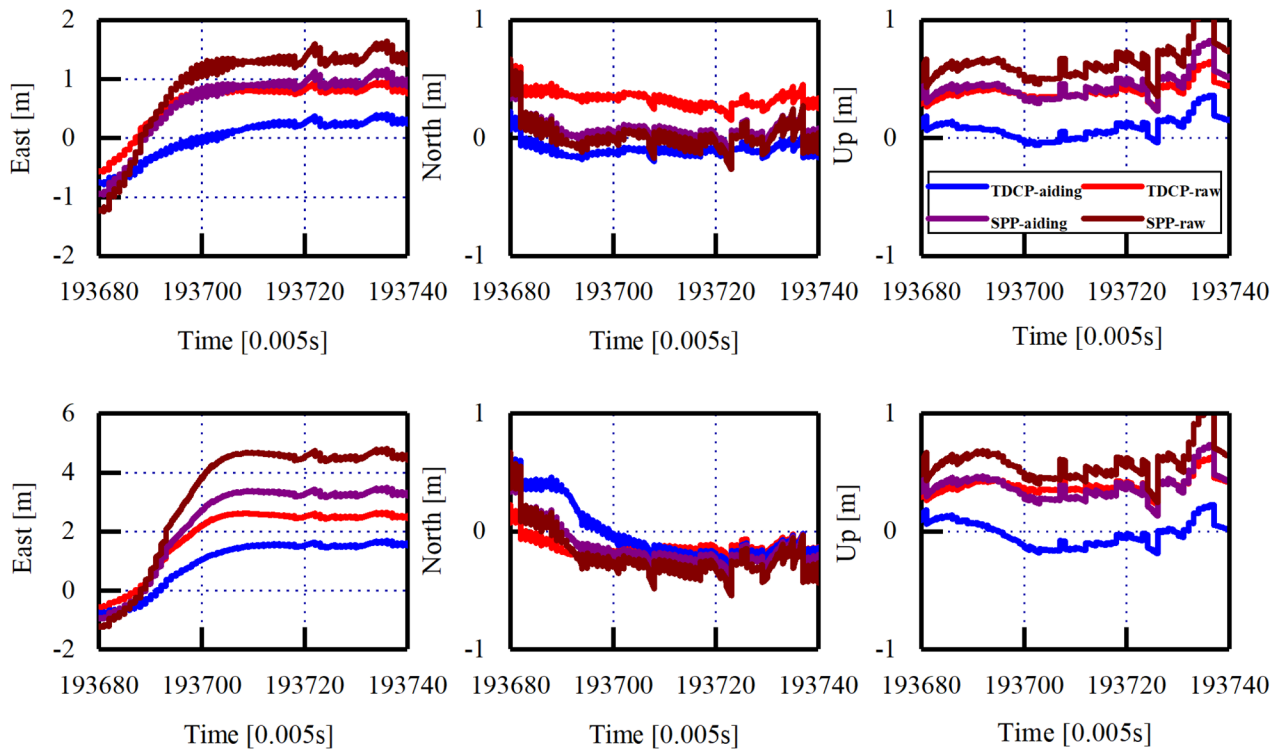
7

Figure 8. Estimated accelerometer bias differences of the SPP-INS (top) and TDCP-INS (bottom) solutions with respect to the reference solution using the RTK-INS tightly coupled system.

Figure 9. Position differences with simulated GPS outages (top: 5 s outages, bottom: 10 s outages).

Figure 10. Trajectory indication under a GNSS-challenged environment. Map data: Google, Maxar Technologies.
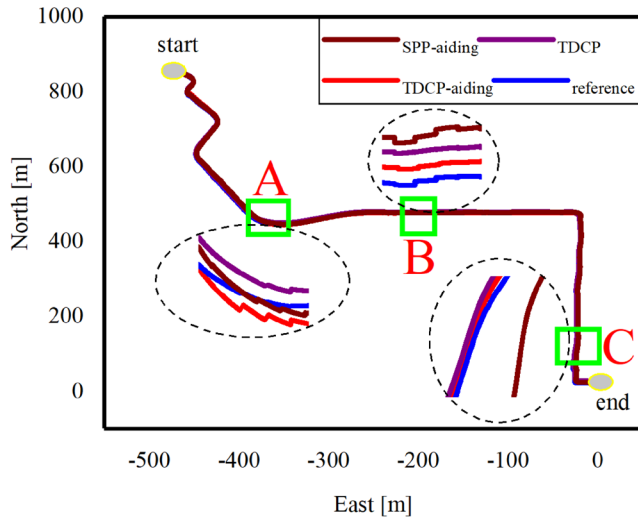

Figure 11. The 2D vehicle trajectory for the TDCP-INS system (green), TDCP-INS with velocity aiding (red), and RTK-INS system (blue) under the GNSS-challenged environment.

Figure 5 shows that the velocity estimates using TDCP measurements are significantly smoother and more accurate than the velocity estimated using the PR-based measurements, which only achieved several meter-level accuracy. Although the TDCP measurements included accurate velocity information, the TDCP-based schemes can obtain cm/s-level accuracy. In the KF with velocity aiding, the variance of the NHC and ODO velocity are assumed to be 0.5^2 m s^{-1} and 1.0^2 m s^{-1}, respectively. Thus, the velocity accuracy of the TDCP-INS with velocity aiding is slightly better than that of the TDCP-INS. The velocity RMSE of the TDCP-INS and TDCP-INS with velocity aiding are approximately 0.0825 m s^{-1}, 0.1209 m s^{-1}, and 0.1453 m s^{-1} in the east, north, and up direction, as shown in table 2.

Equations (9)–(11) show that the NHC improved the velocity and attitude estimations. Figure 6 shows the attitude differences of the SPP-INS, TDCP-INS, and TDCP-INS with velocity aiding. The statistics in table 2 indicate that the attitude RMSE of the TDCP-INS schemes are approximately 0.1432°, 0.1055°, and 1.2354° for the roll, pitch, and yaw directions. Moreover, the accuracy of the yaw component is worse than that of the roll and pitch because of poor observability in the yaw direction compared with the other two directions in the TDCP-INS and SPP-INS schemes. The accelerometer and gyroscope biases are estimated and compensated online in the three schemes. Figures 7 and 8 show the estimated errors.

3.3. Simulate GPS outages test

To evaluate the performance of the TDCP-INS during a GPS outage and show the position performance with INS-only positioning mode, we conducted GPS outage simulations by adding outages of 5 s and 10 s, both beginning at 193 680 s. To demonstrate the improvement in the velocity-aiding method, four schemes were considered: (1) the TDCP-INS during GPS outages (red line), (2) the TDCP-INS with velocity aiding during GPS outages (blue line), (3) the SPP-INS during outages (wine-red line), and (4) the SPP-INS with velocity aiding during GPS outages (purple line). Figure 9 shows the 3D position offsets. We can obtain a position error below 1 m in the TDCP-INS system when the outage time is 5 s with the TDCP-INS mode. However, the position accuracy could worsen to approximately 3 m if the outage time extends to 10 s. During GPS outages, the performance of the TDCP-INS primarily depends on sensor error characteristics. We observe the difference between the red and blue lines, as well as between the wine-red and purple lines in figure 9, which indicates that the performance improved significantly when additional velocity information is included, such that the blue and purple lines are nearly coincidental with the zero line. Comparison between the red and wine-red lines in figure 9 indicates that the TDCP-INS mode performed better than the SPP-INS mode, which benefits from high-accuracy carrier phase measurements. Comparison between the purple and blue lines in figure 9 indicates that the TDCP-INS with velocity aiding performed better than the SPP-INS with velocity aiding during GPS outages. The results shown in figure 9 indicate that the proposed schemes performed better than the classic SPP-INS mode and SPP-INS with velocity constraint, namely additional NHC and ODO information aiding. However, it is worth noting that the TDCP and INS-only mode carried relative information and the position error accumulated during the GPS outages will constantly be retained, even during the GPS signal recovery. Thus, the velocity-aiding algorithm is insufficient to deal with the frequent GNSS signal loss of lock, and the inability to correct the absolute error is a fatal weakness of the TDCP-INS tightly coupled system.

3.4. GPS-challenged environment test

This section evaluates the designed system's performance using data collected from a dense urban area. Figure 10 shows the trajectory of the vehicle, where the start and end points are marked by a yellow circle. During the test, the GPS signal is frequency-sheltered by trees and buildings, which leads to periods of signal blockage. The TDCP is only a relative measurement between consecutive epochs and has no absolute position information included in it. The performance of the TDCP-INS will be poor if the GPS signal is frequency-sheltered, such as in a dense urban area. The velocity-aiding algorithm is insufficient to deal with frequent GNSS signal loss of lock. Thus, to introduce the other absolute position information into the integrated system, the same scheme proposed by

Table 3. The RMSE of the position, velocity, and attitude of the three processing schemes with respect to the reference solution using the RTK-INS tightly coupled system under the GPS-challenged environment.

Mode	Position (m)			Velocity (m s^{-1})			Attitude (deg)		
	East	North	Up	East	North	Up	Roll	Pitch	Yaw
SPP-aiding	2.4883	3.3410	4.8002	1.1064	1.1603	1.4601	0.4891	0.4752	4.8769
TDCP	1.8730	2.0570	2.1080	0.1941	0.2682	0.2673	0.2149	0.2316	2.2050
TDCP-aiding	1.0301	0.7481	1.5290	0.1510	0.2183	0.2043	0.1892	0.1913	1.8289

Han [7] was adopted in this test. That is, PRs are incorporated into the integrated system using a KF with a low update rate to control the accumulation of the system error.

Figure 11 shows the 2D vehicle trajectories for the integrated SPP-INS with aiding (wine-red line), TDCP-INS (purple line), TDCP-INS with velocity aiding (red line), and RTK-INS (blue line) solutions. A, B, and C denote the partial enlargements, and specific statistical information is shown in table 3. In general, after adding PRs, the TDCP-INS system can operate normally without large error drift. The results shown in the partial enlargements A and C are consistent with the findings of the previous test. However, from the partial enlargement A, the TDCP-INS method outperformed the TDCP-INS with velocity aiding, which can be interpreted as NHC, surmising that it does not match the actual result of the vehicle motion. Overall, the dual-rate KF can bound the position drift of the TDCP-INS system. Consistent with the conclusion in section 3.3, the proposed TDCP-INS mode with velocity information aiding performed better than classic SPP-INS mode with velocity constraint, even in a dense urban area. However, due to larger PR noise, the TDCP-INS system with PR absolute positioning accuracy can only achieve SPP accuracy. The statistics shown in table 3 also verified the aforementioned conclusions. From the RMSE perspective, the TDCP-INS with velocity aiding outperformed the TDCP-INS system. The 2D position RMSE improved from 2.782 m to 1.273 m for the TDCP-INS with the velocity-aiding solution for an improvement of 54.2%, which was an improvement of 61.8% compared to SPP-INS with velocity aiding. The improvements in velocity estimates along the east, north, and up directions using TDCP-INS mode with velocity aiding are 86.4%, 81.2%, and 86.0% compared to SPP-INS mode with velocity aiding, respectively. With regards to attitude, the RMSE of roll, pitch and yaw increased by 61.3%, 59.7%, and 62.5%, respectively, compared to SPP-INS mode with velocity aiding. These results show the efficacy of the proposed method.

4. Conclusion

This research presented a velocity-aiding enhanced scheme for a low-cost single-frequency GPS receiver and MEMS-based INS. The scheme aims to improve the positioning performance of the conventional TDCP-INS tightly coupled navigation system. The performance was evaluated in the sky field-of-view and GNSS-challenged environment. The main conclusions from the experimental results are as follows.

(1) The position, velocity, and attitude RMSE of the TDCP-INS are better than those of the SPP-INS, and the positioning accuracy has increased by an order of magnitude.
(2) TDCP measurements only carry relative positioning information, which could introduce position error accumulation without absolute position aiding. After velocity aiding, the position drift of the TDCP-INS will be bound, and the INS error will be reduced during GNSS outages.
(3) The TDCP-INS tightly coupled schemes with velocity aiding achieved improvements of approximately 7.8%, 17.8%, and 3.7% in the east, north, and up directions, respectively, under the sky field-of-view test.
(4) Frequent signal loss of lock will introduce a large position drift into the TDCP-INS system, and a velocity-aiding algorithm will be insufficient to deal with frequent GNSS outages. Special considerations are required to provide accurate absolute positioning information. The TDCP-INS system included PR measurements that could only achieve SPP accuracy. The 2D position accuracy improved after the velocity-aiding solution with an improvement of 52.4% under the GNSS-challenged environment.

Lastly, this study aims for a low-cost integrated navigation system, which only needs to meet meter-level positioning accuracy. Thus, the proposed TDCP-INS with velocity aiding has a certain practical significance for low-accuracy applications compared with the SPP-INS.

ORCID iDs

Guobin Chang ⬤ https://orcid.org/0000-0001-6392-3265

References

[1] Shin E-H 2001 *Accuracy Improvement of Low Cost INS/GPS for Land Applications* (Canada: Univ. Calgary)

[2] Noureldin A, Karamat T B and Georgy J 2012 *Fundamentals of Inertial Navigation, Satellite-Based Positioning and Their Integration* (Berlin: Springer)

[3] Gu Y, Hsu L T and Kamijo S 2016 GNSS/Onboard inertial sensor integration with the aid of 3D building map for lane-level vehicle self-localization in urban canyon *IEEE Trans. Veh. Technol.* **65** 4274–87

[4] Wei J, Yong L and Rizos C 2013 On-the-fly Locata/inertial navigation system integration for precise maritime application *Meas. Sci. Technol.* **24** 105104

[5] Zhao L and Quan H 2019 Using regularized softmax regression in the GNSS/INS integrated navigation system with nonholonomic constraints *IOP Conf. Series: Materials Science and Engineering* (Bristol: IOP Publishing) p 012058

[6] Chen W, Li X, Song X, Li B, Song X and Xu Q 2015 A novel fusion methodology to bridge GPS outages for land vehicle positioning *Meas. Sci. Technol.* **26** 075001

[7] Han S and Wang J 2012 Integrated GPS/INS navigation system with dual-rate Kalman filter *GPS Solut.* **16** 389–404

[8] Wendel J, Meister O, Monikes R and Trommer G 2006 Time-differenced carrier phase measurements for tightly coupled GPS/INS integration *2006 IEEE/ION Position, Location, And Navigation Symp.* (IEEE) pp 54–60

[9] Soon B K, Scheding S, Lee H-K, Lee H-K and Durrant-Whyte H 2008 An approach to aid INS using time-differenced GPS carrier phase (TDCP) measurements *GPS Solut.* **12** 261–71

[10] Han H, Wang J, Wang J and Tan X 2015 Performance analysis on carrier phase-based tightly-coupled GPS/BDS/INS integration in GNSS degraded and denied environments *Sensors* **15** 8685–711

[11] Li T, Zhang H, Niu X and Gao Z 2017 Tightly-coupled integration of multi-GNSS single-frequency RTK and MEMS-IMU for enhanced positioning performance *Sensors* **17** 2462

[12] Liu S, Sun F, Zhang L, Li W and Zhu X 2016 Tight integration of ambiguity-fixed PPP and INS: model description and initial results *GPS Solut.* **20** 39–49

[13] Rabbou M A and El-Rabbany A 2015 Tightly coupled integration of GPS precise point positioning and MEMS-based inertial systems *GPS Solut.* **19** 601–9

[14] Paziewski J 2015 Precise GNSS single epoch positioning with multiple receiver configuration for medium-length baselines: methodology and performance analysis *Meas. Sci. Technol.* **26** 035002

[15] Zhu F, Hu Z, Liu W and Zhang X 2019 Dual-antenna GNSS integrated with MEMS for reliable and continuous attitude determination in challenged environments *IEEE Sens. J.* **19** 3449–61

[16] Henkel P and Zhu C 2011 Carrier phase integer ambiguity resolution with inequality constraints for GPS and Galileo *2011 IEEE Statistical Signal Processing Workshop (SSP)* (IEEE) pp 409–12

[17] Han H and Wang J 2017 Robust GPS/BDS/INS tightly coupled integration with atmospheric constraints for long-range kinematic positioning *GPS Solut.* **21** 1285–99

[18] Han H, Wang J, Wang J and Moraleda A H 2017 Reliable partial ambiguity resolution for single-frequency GPS/BDS and INS integration *GPS Solut.* **21** 251–64

[19] Yang L, Li Y, Wu Y and Rizos C 2014 An enhanced MEMS-INS/GNSS integrated system with fault detection and exclusion capability for land vehicle navigation in urban areas *GPS Solut.* **18** 593–603

[20] Chen C, Chang G, Luo F and Zhang S 2019 Dual-frequency carrier smoothed code filtering with dynamical ionospheric delay modeling *Adv. Space Res.* **63** 857–70

[21] Chang G 2014 On Kalman filter for linear system with colored measurement noise *J. Geodesy* **88** 1163–70

[22] Zhao Y 2015 Cubature + extended hybrid Kalman filtering method and its application in PPP/IMU tightly coupled navigation systems *IEEE Sens. J.* **15** 6973–85

[23] Zhao Y 2017 Applying time-differenced carrier phase in nondifferential GPS/IMU tightly coupled navigation systems to improve the positioning performance *IEEE Trans. Veh. Technol.* **66** 992–1003

[24] Niu X, Cheng Y and Shi C 2012 Observability analysis of non-holonomic constraints for land-vehicle navigation systems *J. Glob. Position. Syst.* **11** 80–8

[25] Juang J C and Lin C F 2015 A sensor-fusion scheme for the estimation of vehicular speed and heading angle *IEEE Trans. Veh. Technol.* **64** 2773–82

[26] Godha S and Cannon M 2007 GPS/MEMS INS integrated system for navigation in urban areas *GPS Solut.* **11** 193–203

[27] Zhou F, Dong D, Li W, Jiang X, Wickert J and Schuh H 2018 GAMP: an open-source software of multi-GNSS precise point positioning using undifferenced and uncombined observations *GPS Solut.* **22** 33